CODEN IEJMAT *Internet Electronic Journal of Molecular Design* **2007**, *6*, 237–252 ISSN 1538–6414
BioChem Press http://www.biochempress.com

Inter*net* Electronic Journal of Molecular Design

August 2007, Volume 6, Number 8, Pages 237–252

Editor: Ovidiu Ivanciuc

Three–Dimensional Quantitative Structure–Activity Relationship (3D–QSAR) Studies of Various Ether Analogues of Farnesyltransferase Inhibitors

Tabish Equbal,[1] Om Silakari,[1] and Muttineni Ravikumar [2]

[1] Department of Pharmaceutical Science and Drug Research, Punjabi University, Patiala 147–002, Punjab, India
[2] GVK Biosciences Pvt. Ltd., #210 'My Home Tycoon', 6–3–1192 Begumpet, Hyderabad 500 016, India

Received: December 12, 2006; Revised: February 12, 2006; Accepted: April 7, 2006; Published: August 31, 2007

Citation of the article:
T. Equbal, O. Silakari, and M. Ravikumar, Three–Dimensional Quantitative Structure–Activity Relationship (3D–QSAR) Studies of Various Ether Analogues of Farnesyltransferase Inhibitors, *Internet Electron. J. Mol. Des.* **2007**, *6*, 237–252, http://www.biochempress.com.

Copyright © 2007 BioChem Press

Inter*net* Electronic Journal of Molecular Design

BioChem Press
http://www.biochempress.com

Three–Dimensional Quantitative Structure–Activity Relationship (3D–QSAR) Studies of Various Ether Analogues of Farnesyltransferase Inhibitors

Tabish Equbal,[1] Om Silakari,[1,*] and Muttineni Ravikumar[2]

[1] Department of Pharmaceutical Science and Drug Research, Punjabi University, Patiala 147–002, Punjab, India

[2] GVK Biosciences Pvt. Ltd., #210 'My Home Tycoon', 6–3–1192 Begumpet, Hyderabad 500 016, India

Received: December 12, 2006; Revised: February 12, 2006; Accepted: April 7, 2006; Published: August 31, 2007

Internet Electron. J. Mol. Des. **2007**, *6* (8), 237–252

Abstract

Motivation. The inhibition of farnesyltransferase (FTase) has been vigorously pursued as a promising target for the treatment of a broad spectrum of cancers. A set of hundred ether analogues reported as farnesyltransferase inhibitors (FTIs) were analyzed by employing the molecular field analysis (MFA) technique to investigate the structural requirements for various ether analogues to inhibit FTase and to derive a highly predictive model that may be used for the designing of novel FTIs.

Method. MFA is one of the popular 3D–QSAR methods that relate biological activity of molecules with steric and electrostatic fields on a rectangular grid around a bundle of active molecules. MFA studies were performed with the QSAR module of Cerius^2 using genetic partial least squares (G/PLS) algorithm.

Results. The MFA model was established from the training set of 80 molecules and validated by predicting the activities of 20 test set molecules. The analysis has produced statistically significant and reasonably predictive QSAR model with $r = 0.919$, $r^2 = 0.846$, $r^2_{cv} = 0.785$, $r^2_{pred} = 0.714$. The MFA model was cross–validated with the leave–one–out (LOO) method.

Conclusions. The 3D–QSAR models have good correlation and predictive ability. The model showed that steric (CH_3) and electrostatic (H^+) interaction play important role in the inhibition of FTase by ether analogues. The model generated can be exploited for structural modification in order to improve FTase inhibition.

Keywords. Farnesyltransferase; 3D–QSAR; MFA; molecular field analysis; anti–cancer; farnesyltransferase inhibitors.

Abbreviations and notations

FPP, farnesyl diphosphate	MFA, molecular field analysis
FTase, farnesyltransferase	MCSG, maximum common subgroup
FTIs, farnesyltransferase inhibitors	PLS, partial least squares
GFA, genetic function approximation	PRESS, predicted sum of squares
G/PLS, genetic partial least squares	3D–QSAR, three–dimensional quantitative structure–activity relationships

Dedicated to Professor Lemont B. Kier on the occasion of the 75th birthday.

* Correspondence author; E–mail: omsilakari@rediffmail.com.

1 INTRODUCTION

Farnesyltransferase (FTase) has become a major target in the development of potential anti–cancer drugs. It has been shown that farnesyltransferase inhibitors (FTIs) can stop protein farnesylation and suppress the growth of Ras dependent tumor cells. FTase is a zinc metalloenzyme which catalyzes the reaction between farnesyl diphosphate (FPP) and the cysteine residue found in the tetrapeptide sequence CAAX (C = Cys, A = an aliphatic amino acid, X is typically Met) in the carboxyl terminal of a group of membrane–bound small G–proteins such as Ras, RhoB, RhoE, lamin A and B, and transducin [1]. Hence, over the last two decades, several researchers synthesized different class of FTIs, such as SCH66336 (Sarasar^{TM}) and R115777 (tipifarnib or Zanestra^{TM}) are currently used in advanced human clinical trials [2–4]. FTIs are promising agents in cancer therapy due to their excellent efficacy and low systemic toxicity in pre–clinical animal models.

Very often, in ligand design one determines the experimental activity for the interaction between a ligand and a receptor without any information on the structure of the biological target. Using the experimental activity for a set of compounds that have an affinity for the active site, one can generate a virtual receptor site that models the ligand receptor interactions [5–10]. A three–dimensional quantitative structure activity relationship (3D–QSAR) equation based on virtual receptor model should give reliable prediction that can guide the synthesis of new compounds with a good affinity for the investigated receptor.

The present study aimed at elucidating the structural features required for FTase inhibition and to obtain predictive 3D–QSAR model, which may guide the rational synthesis of novel inhibitors. The 3D–QSAR model was generated using the one of the popular computational methods, molecular field analysis (MFA) [11–12] for a series of various ether analogues of FTIs. This MFA model would give insight to the influence of various interactive fields on the activity and thus, can help in designing and forecasting the FTase inhibitory activity of novel molecules.

2 MATERIALS AND METHODS

2.1 Data Set

The data sets of 100 ether analogues were selected and FTase inhibitory activity data (IC_{50}) was collected from literature [13–15]. The data set was divided into training set (80 molecules) and test set (20 molecules). Biological activities were converted into the corresponding pIC_{50} values (–log IC_{50}), where IC_{50} value represents the drug in molar concentration that causes 50% inhibition of FTase. The pIC_{50} values of the molecules under study spanned a wide range from 6 to 10. All the IC_{50} values were obtained using the same assay method [16]. The structures and biological activity data of training and test set molecules are described in Tables 1.

2.2 Molecular Modeling

Molecular modeling analysis was performed using Cerius^2 software [17]. The structures of the compounds were built using molecular sketcher facilities provided in the modeling environment of Cerius^2. Geometric optimization was carried using DREIDING force field [18]. Partial atomic charges were calculated using the Gasteiger method [19]. Multiple conformations of each molecule were generated using the Boltzmann Jump as a conformational search method to obtain lowest energy conformation. All molecules were initially energy minimized with smart minimizer option in Cerius^2 software. Further geometric optimization of each molecule was carried out with MOPAC 6 package using the semi–empirical AM1 (Austin Model) Hamiltonian [20].

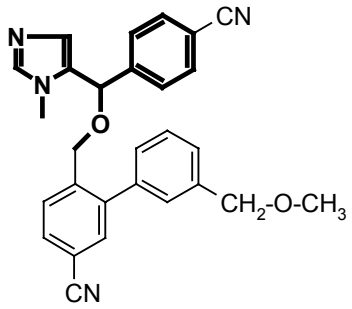

Figure 1. The bold faced portion of the most active molecule **13** was used as the template for the superimposition of the rest of the molecules.

2.3 Molecular Alignment

A proper alignment of the structures is critical for obtaining valid 3D–QSAR models. Furthermore, it is vital that all compounds are aligned in a pharmacological active orientation since the 3D–QSAR model assumes that each structure exhibits activity at the same binding site of the receptor. To obtain a consistent alignment, all the molecules were superimposed on to the shape reference compounds, which were selected as a conformer of the most active molecules. The method used for performing the alignment was the maximum common subgroup (MCSG) method [17]. This method looks at molecules as points and lines, and uses the techniques of graph theory to identify patterns. It finds the largest subset of atoms in the shape reference compound that is shared by all the structures in the study table and uses this subset for alignment. A rigid fit of atom pairings was performed to superimpose each structure so that it overlays the shape reference compound. The bold–faced portion of the most active molecule **13** shown in Figure 1 was used as the template for the superimposition. The stereoview of aligned molecules is shown in Figure 2.

2.4 Molecular Field Analysis

All the studies were performed with the QSAR module of Cerius^2. MFA model is predictive and sufficiently reliable to guide the chemist in the design of novel compounds. This approach is effective for the analysis of data sets where activity information is available but the structure of the

receptor site is unknown. It attempts to postulate and represent the essential features of a receptor site from the aligned common features of the molecules that bind to it. The MFA calculates probe interaction energies on a rectangular grid around a bundle of active molecules. The atomic coordinates of the contributing models are used to compute field values on each point of a 3D grid. Fields of molecules are represented using grids in MFA and each energy associated with an MFA grid point can serve as input for the calculation of a QSAR. These energies were added to the study table to form new columns headed according to the probe type. The molecular field was created using proton and methyl groups as probes, which represent electrostatic and steric fields, respectively. Only 10% of the total descriptors whose variance was highest were considered for further analysis. The major steps of molecular field analysis were (1) Generate conformers and energy minimization; (2) Match atoms using maximum common subgroup (MCSG) search and aligning molecules using default option; (3) Set MFA preferences (rectangular grid with 2 Å step size, charges by Gasteiger algorithm, H^+ and CH_3 as probes); (4) Compute the field; and (5) Regression analysis by genetic partial least squares (G/PLS) [17] algorithm.

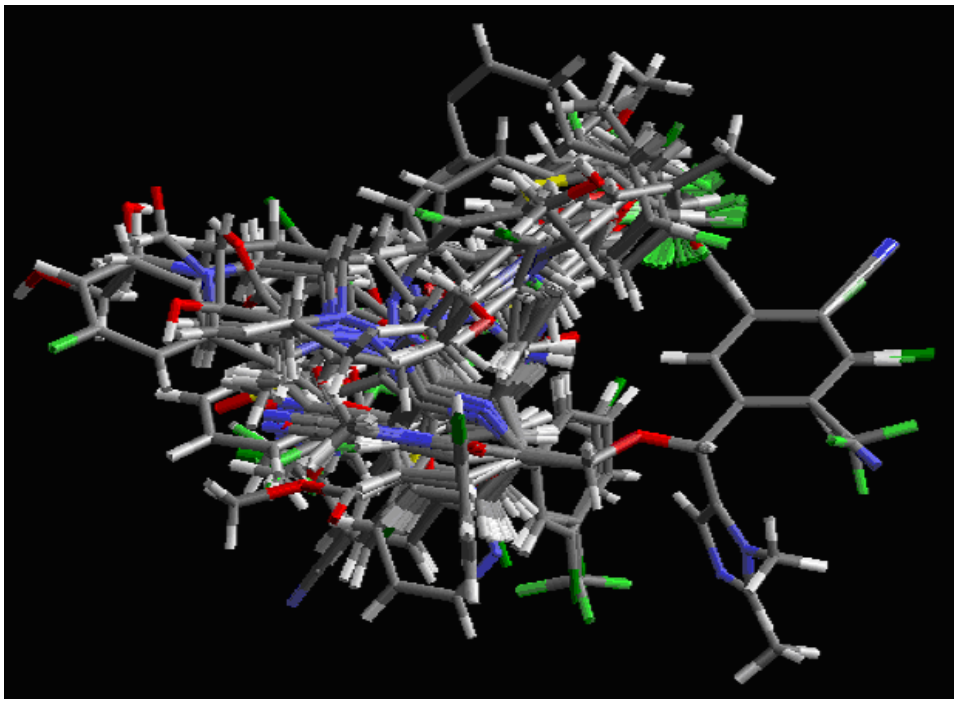

Figure 2. The stereoview of aligned molecules of the training set.

2.5 Genetic Partial Least Squares (G/PLS)

The regression analysis of data was performed using G/PLS techniques available in QSAR+ environment of Cerius[2] software. This algorithm may be used as an alternative to a genetic function approximation (GFA) calculation. G/PLS is derived from two QSAR calculation methods: GFA and partial least squares (PLS). Both GFA and PLS have been shown to be valuable tools in cases where the data set has more descriptors than samples. The G/PLS algorithm uses GFA to select

appropriate basis functions to be used in a model of the data and PLS regression as the fitting technique to weigh the basis functions relative contributions in the final model. PLS is a generalization of regression, which can handle data with strongly correlated and/or noisy or numerous X variables [21]. It gives a reduced solution, which is statistically more robust than multiple linear regression (MLR). The linear PLS model finds "new variables" (latent variables or X scores) which are linear combinations of the original variables. To avoid overfitting, a strict test for the significance of each consecutive PLS component is necessary and then stopping when the components are not significant. Cross–validation is a practical and reliable method of testing this significance [22].

Table 1. The structures and inhibitory activity data for the training and test set molecules of FTIs

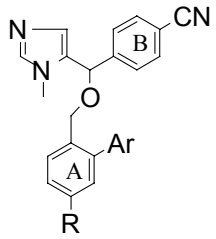

Compound no.	R	Ar	IC_{50} (nM) [a]	Experimental activity [b] pIC_{50}	Predicted activity [c] pIC_{50}
1	Cl	3–Cl–Ph	0.80	9.096	8.607
2	Cl	4–Cl–Ph	4.8	8.318	8.609
3	Cl	3–OMe–Ph	0.91	9.040	8.643
4	Cl	3–OEt–Ph	1.1	8.958	9.063
5	CN	Ph	1.3	8.886	8.743
6	CN	1–naphthyl	0.94	9.026	8.982
7*	CN	8–quinolinyl	5.2	8.283	8.329
8	CN	3–Cl–Ph	0.87	9.060	8.926
9	CN	3–OMe–Ph	0.75	9.455	9.201
10	CN	3,4–OCH_2O–Ph	0.87	9.060	8.716
11	CN	3,4–OCF_2O–Ph	1.1	8.958	8.862
12	CN	3–OEt–Ph	0.69	9.161	9.164
13	CN	3–CH_2OCH_3–Ph	0.19	9.721	9.188
14	CN	4–OMe–Ph	0.96	9.017	9.195
15*	CN	4–OEt–Ph	1.2	8.920	9.101
16	CN	4–OCF_3–Ph	0.84	9.075	9.520
17*	CN	4–CH_3–Ph	1.1	8.958	8.980
18	CN	3,5–DiF–Ph	0.98	9.008	9.121
19	NO_2	3–OMe–Ph	1.1	8.958	8.940
20	NH_2	3–OMe–Ph	40	7.397	7.823
21*	$NHSO_2CH_3$	3–OMe–Ph	35	7.455	7.734
22	$NHCOCH_2OMe$	3–OMe–Ph	11	7.958	8.320
23	CO_2Me	3–OMe–Ph	13	7.886	7.924
24	CHO	3–OMe–Ph	1.6	8.795	8.953

[a] IC_{50} values collected from literature (Reference [13–15])
[b] $pIC_{50} = -\log IC_{50} = \log 1/IC_{50}$
[c] pIC_{50} predicted from best model (equation 1)
*Test set

Table 1. (Continued)

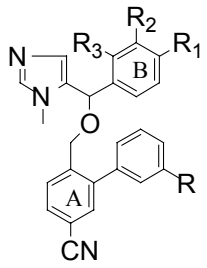

Compound no.	R	R_1	R_2	R_3	IC_{50} (nM)	Experimental activity pIC_{50}	Predicted activity pIC_{50}
25	OMe	Cl	H	H	2.0	8.698	8.573
26*	OMe	CN	Cl	H	0.97	9.013	8.547
27	Cl	CN	F	H	0.44	9.356	9.205
28	Cl	CN	H	F	0.77	9.113	9.127
29	Cl	CF_3	H	H	1.1	8.958	9.009

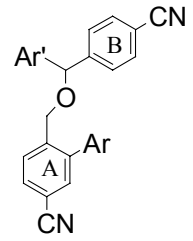

Compound no.	Ar'	Ar	IC_{50} (nM)	Experimental activity pIC_{50}	Predicted activity pIC_{50}
30	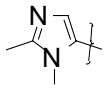	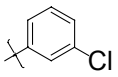	2.0	8.698	9.027
31*	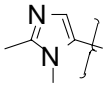	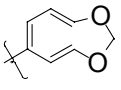	1.6	8.795	9.047

Table 1. (Continued)

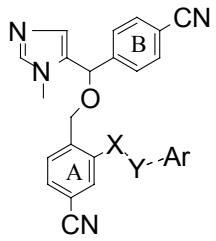

Compound no.	X–Y	Ar	IC_{50} (nM)	Experimental activity pIC_{50}	Predicted activity pIC_{50}
32*	$NHSO_2$		0.88	9.055	8.623
33	$NHSO_2$	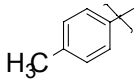	1.0	9.000	8.687
34	$NHSO_2$	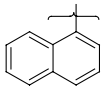	2.6	8.585	8.885
35*	$NHCH_2$	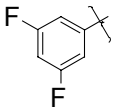	0.61	9.214	8.464
36	NHCO		5.0	8.301	8.455
37	CONH		2.2	8.657	8.919
38	CONH	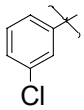	0.75	9.124	8.843

Table 1. (Continued)

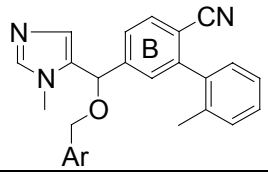

Compound no.	Ar (Ring A)	IC_{50} (nM)	Experimental activity pIC_{50}	Predicted activity pIC_{50}
39	Phenyl	84	7.075	7.386
40	o–Tolyl	54	7.267	7.380
41	m–Tolyl	61	7.214	7.226
42	p–Tolyl	54	7.267	7.188
43	p–^{i}pr–phenyl	51	7.292	7.217
44	p–^{t}Bu–phenyl	87	7.060	6.933
45	p–phenyl–phenyl	13	7.886	7.579
46*	1–Naphthyl	17	7.769	7.387
47	2–Naphthyl	65.7	7.181	7.352
48	8–Quinolyl	59	7.229	7.305
49*	p–Methoxyphenyl	59	7.229	7.788
50	m–F_3CO–phenyl	8.3	8.080	7.583
51	p–F_3CO–phenyl	16	7.795	7.603
52	m–F_3C–phenyl	8.1	8.091	8.080
53	p–F_3C–phenyl	12	7.920	8.103
54*	o–Cyano–phenyl	62	7.207	7.760
55	m–Cyano–phenyl	18	7.744	7.698
56	p–Cyano–phenyl	4	8.397	8.220
57	p–F–phenyl	32	7.494	7.600
58*	o–Cl–phenyl	48	7.318	7.221
59	m–Cl–phenyl	19	7.721	7.655
60*	p–Cl–phenyl	11	7.958	8.110
61	o–Br–phenyl	76.9	7.113	6.909
62	m–Br–phenyl	13	7.886	8.046
63	p–Br–phenyl	12	7.920	7.958
64	p–NO_2–phenyl	7.5	8.124	8.402
65	m–CO_2CH_3–phenyl	61	7.214	7.572
66	p–CO_2CH_3–phenyl	6.1	8.214	7.502
67	p–CH_3SO_2–phenyl	38	7.420	7.374
68	3,4–Cl,Cl–phenyl	27	7.568	7.581
69	3,5–Cl,Cl–phenyl	19	7.721	7.752
70	2,6–Cl,Cl–phenyl	81	7.091	7.534
71	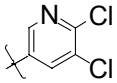	15	7.823	7.967
72*	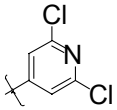	13	7.886	8.068
73	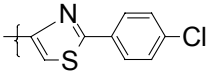	29	7.537	7.686
74	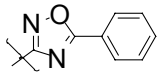	89.2	7.049	7.440
75*	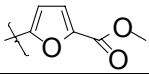	100	7.000	6.305

Table 1. (Continued)

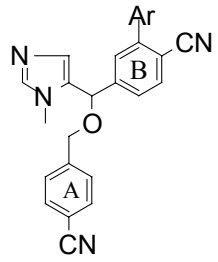

Compound no.	Ar	IC_{50} (nM)	Experimental activity pIC_{50}	Predicted activity pIC_{50}
76*	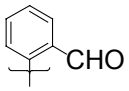	1.9	8.721	8.252
77	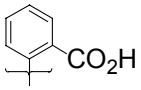	14	7.853	8.312
78	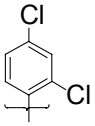	47	7.327	7.668
79	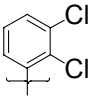	1.5	8.823	8.515
80	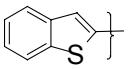	160	6.795	6.941

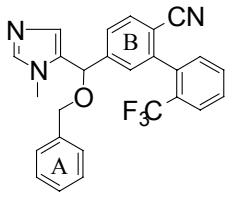

Compound no.	Ar (Ring A)	IC_{50} (nM)	Experimental activity pIC50	Predicted activity pIC50
81	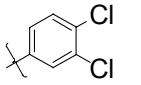	1.7	8.769	8.140
82	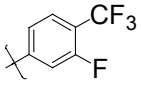	6.1	8.214	8.281
83*	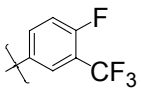	4.1	8.387	8.127
84	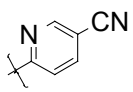	2.7	8.568	8.260
85	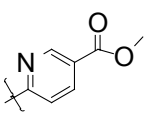	9	8.045	7.808

Table 1. (Continued)

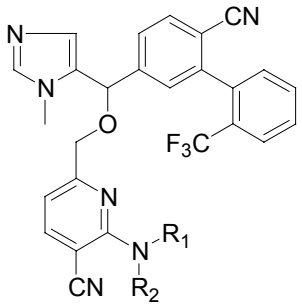

Compound no.	R_1R_2N–	IC_{50} (nM)	Experimental activity pIC_{50}	Predicted activity pIC_{50}
86	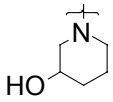	1.3	8.886	8.419
87		3.6	8.443	8.300
88	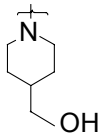	1.8	8.744	8.747
89*	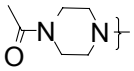	2.6	8.585	9.220
90*	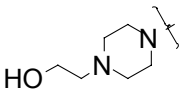	1.3	8.886	8.936
91	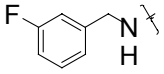	10	8.000	8.413

Table 1. (Continued)

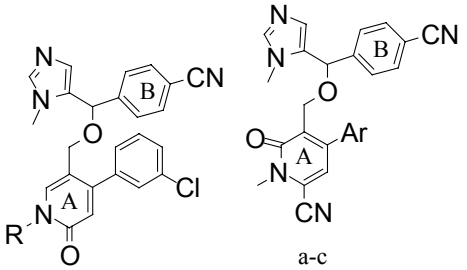

a-c

Compound no.	Ar	R	IC_{50} (nM)	Experimental activity pIC_{50}	Predicted activity pIC_{50}
92(**a**)	3–Cl–Ph	–	1.2	8.920	8.353
93(**b**)	3,5–Di–Cl–Ph	–	1.1	8.958	8.751
94(**c**)	3–CF_3–Ph	–	7.5	8.124	8.282
95	–	H	11	7.958	8.639
96	–	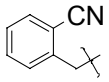	2.3	8.638	8.854
97	–	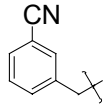	1.3	8.886	9.074
98	–	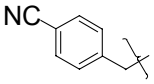	5.0	8.301	8.492
99*	–	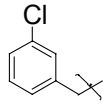	2.1	8.677	8.707
100	–	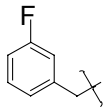	2.1	8.677	8.298

The QSAR application of G/PLS thus allows the construction of larger models while still avoiding overfitting and eliminating most variables. Best model was selected based on statistical measures such as number of data points (*n*), correlation coefficient (*r*), square correlation coefficient (r^2), cross–validated correlation coefficient (r^2_{cv}), predicted correlation coefficient (r^2_{pred}), predicted sum of squares (*PRESS*), bootstrap correlation coefficient (r^2_{BS}).

3 RESULTS AND DISCUSSION

Equation 1 is the best model developed for 80 training set molecules. In this equation, the steric (CH_3) and electrostatic (H^+) descriptors specify the regions where variations in the structural features (steric or electrostatic) of different compounds in the training set, lead to increased or decreased activities. The number accompanying descriptors represents its position in the three–dimensional MFA grid. For present study, G/PLS was carried out over 50,000 generations with a population size of 100. The optimal number of components was set to 5. An energy cutoff of –30 to

+30 kcal/mol was set for both steric and electrostatic contributions. Cutoff energy difference of 30 kcal/mol was chosen because this limit allows sampling an exhaustive amount of torsion angle space in which an active conformation, if present, should be found. The smoothing parameter, d was set to 1.0 to control the bias in the scoring factors between equations with different number of terms. The length of the final equation was fixed to nine terms. The cross–validation was performed with the leave–one–out procedure. PLS analysis was scaled, with all variables normalized to a variance of 1.0. The statistical results of the best MFA model are given in equation 1. The numbers associated with the descriptor specify its location in the 3D–grid around the molecule as shown in Figure 4.

$$\begin{gathered}\text{Activity} = 7.795 - 0.04303(H^+/526) - 0.036992(CH_3/1165) + 0.015616(H^+/1142) \\ + 0.036366(CH_3/1319) + 0.023058(H^+/1465) + 0.071102(CH_3/999) \\ - 0.013647(H^+/1014) - 0.01055(H^+/974) \\ n = 80 \quad r = 0.919 \quad r^2 = 0.846 \quad r^2_{cv} = 0.785 \quad PRESS = 8.936 \\ N = 5 \quad r^2_{pred} = 0.714 \quad r^2_{BS} = 0.830 \quad LSE = 0.080\end{gathered} \tag{1}$$

From these results, it can be observed that Eq. (1) is of good statistical quality. It explains 84.6% variation in the activity with respect to steric and electrostatic fields while leave–one– out cross–validation power of prediction is 78.5%. An *r* is a relative measure of the quality of fit of the model. Its value depends on the overall variance of the data. A QSAR equation can be accepted if the correlation coefficient is around or better then 0.9, equation 1 has the high *r* value of 0.919. An r^2, the square of the correlation coefficient, which is used to describe the goodness of fit of the data of the study compounds to the QSAR model and obtained model has a good correlation coefficient of 0.846. An r^2_{cv}, a squared correlation coefficient generated during a validation procedure, used as a diagnostic tool to evaluate the predictive power of an equation. Cross–validation is often used to determine how large a model (number of terms) can be used for a given data set and the generated model has good cross validation of 0.785. An r^2_{BS} value of 0.830 is the average squared correlation coefficient calculated during the validation procedure. An r^2_{BS} is computed from the subset of variables used one at a time for the validation procedure. Activity of the training set molecules were predicted using this equation and shown in Table 1 and Figure 3(*a*).

A high value of r^2_{cv} alone, however, is an insufficient criterion for a QSAR model to be robust and highly predictive [23]. Once the desired MFA has been constructed, the predictive power of the model was validated with the 20 test set molecules. The predictive power of the model generated, is calculated by Eq. (2):

$$r^2_{pred} = (SD–PRESS)/SD \tag{2}$$

where *SD* is the sum of squared deviations between biological activities of each molecule and the mean activity of the training set molecules and *PRESS* is the sum of squared deviations between the predicted and experimental activity values for every molecule in the test set. The prediction of the model was reasonably good with a predictive correlation coefficient (r^2_{pred}) value of 0.713 and is

shown in Figure 3(*b*).

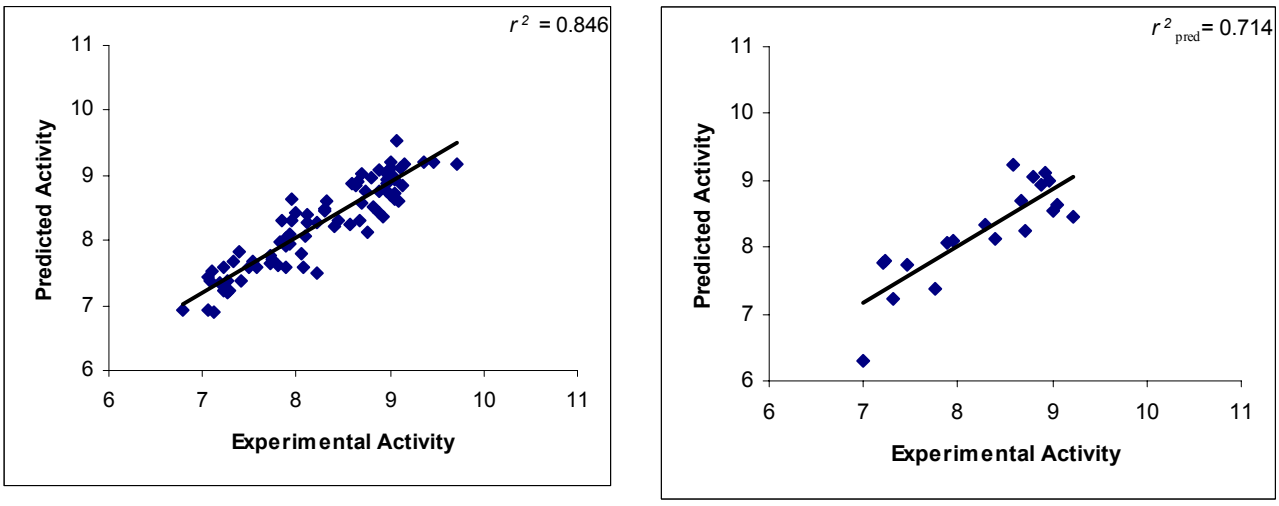

(*a*) (*b*)

Figure 3. Predicted versus experimental activity for training set (*a*) and test set (*b*) for the best MFA model.

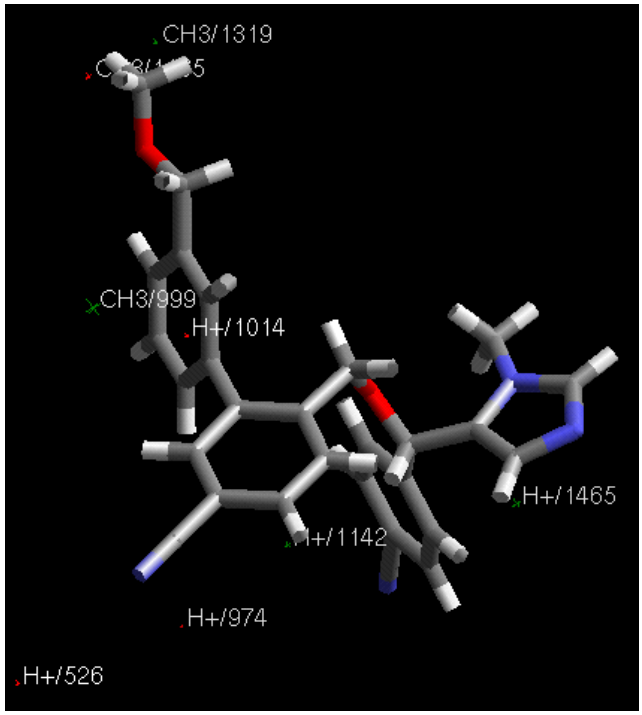

Figure 4. The stereoview of MFA model and the interaction points. The most active compound **13** is displayed in background as reference.

The stereoview of the best model corresponding to equation 1 is shown in Figure 4. Appearance of steric descriptor (CH_3/1319) and (CH_3/999) with positive co–efficient and presence of (CH_3/1165) with negative coefficient indicates moderately bulky substituents would be favorable at *meta* and *para* position of the aromatic ring which is present at *ortho* position of the ring 'A'. Therefore, molecule **13** (Figure 4) showed higher activity as compare to molecules **5**, **6**, **8**, **14**, and

16. The presence of (H^+/1142) with positive coefficient indicates electron–withdrawing group at *meta* position of the ring 'A' is favorable for the activity. Hence, molecule **50**, **52**, **59**, **62**, **69**, **92**(**a**), **93**(**b**), and **94**(**c**) show higher activity as compare to molecules **41**.

The presence of (H^+/1465) with positive coefficient indicates electron withdrawing group increases the activity at *meta* position of the ring 'B', hence molecule **27** having fluorine shows higher activity as compare to molecules **25**, **28**, and **29**.

4 CONCLUSIONS

MFA models are quantitative and differ from pharmacophore models [24, 25], which are qualitative, in that the former tries to capture essential information about the receptor, while the latter only captures information about the similarity of the compounds that bind. MFA attempts to postulate and represent the essential features of a receptor site itself, rather than the common features of the molecules that bind to it. The MFA application uses 3D surfaces that define the shape of the receptor site. The global minimum of the most active compound **13** in the study compounds (based on the value in the activity column) was made as the active conformer. When there is no information on the actual "active conformation" of the ligands, MFA does not really describe the receptor; it describes a self–consistent field around the molecules that can explain activity. It really is just one of possibly many self–consistent models that fit the biological activity data. This model ought to be predictive and sufficiently reliable to guide the chemist in the design of novel compounds. This approach is effective for the analysis of data sets where activity information is available but the structure of the receptor site is unknown.

3D–QSAR method, *i.e.*, MFA, was applied to rationalize the FTase activity of a set of 100 molecules belonging to the various ether analogous. The model was generated with training set of 80 molecules and having a high correlation coefficient, r^2 of 0.846 and with a good cross–validated correlation coefficient, r^2_{cv} of 0.785. The predictive ability of the model was validated using 20 test set molecules and obtained a good r^2_{pred} of 0.714. The significant predictive ability of the MFA model observed for the external test set molecules supports that derived models can be used for the designing of the novel inhibitors. All the 3D features (*i.e.*, electrostatic and steric) can be easily identified from the maps generated for best model and the substitutional requirements can be identified for the favorable interaction with FTase. Overall, the present MFA study investigate the indispensable structural features of the various ether analogues molecules which can be exploited for the structural modifications of these lead molecules in order to achieve improved FTase inhibitory activity.

Acknowledgment

The authors thanks to the Head, Dr. A. K. Tiwary, Department of Pharmaceutical Science and Drug Research, for their steady advice and helpful collaborations and Dr. J.A.R.P. Sarma, Director, Bioinformatics division, GVK Biosciences Pvt. Ltd. for providing software facilities and giving a great chance to work there.

5 REFERENCES

[1] F. L. Zhang and P. Casey, Protein Prenylation: Molecular Mechanisms and Functional Consequences, *J. Annu. Rev. Biochem*. **1996**, *65*, 241–269.
[2] I. M. Bell, Inhibitors of Farnesyltransferase: A Rational Approach to Cancer Chemotherapy, *J. Med. Chem*. **2004**, *47*, 1869–1878.
[3] S. Ayral–Kaloustian and E. Salaski, Protein Farnesyltransferase inhibitors, *Curr. Med. Chem*. **2002**, *9*, 1003–1032.
[4] A. A. Adjei, *Drugs Future* **2000**, *25*, 1069–1079.
[5] O. Ivanciuc, 3D QSAR Models; In: *QSPR/QSAR Studies by Molecular Descriptors*, Ed.: M. V. Diudea, Nova Science Publishers, Huntington, NY, 2001, pp. 233–280.
[6] O. Ivanciuc, T. Ivanciuc, D. Cabrol–Bass, Comparative Receptor Surface Analysis (CoRSA) Model for Calcium Channel Antagonists, *SAR QSAR Environ. Res*. **2001**, *12*, 93–111.
[7] O. Ivanciuc, T. Ivanciuc, D. Cabrol–Bass, 3D Quantitative Structure Activity Relationships with CoRSA. Comparative Receptor Surface Analysis. Application to Calcium Channel Agonists, *Analusis* **2000**, *28*, 637–642.
[8] A. Hirashima, T. Eiraku, E. Kuwano, E. Taniguchi, and M. Eto, Three–dimensional Pharmacophore Hypotheses of Octopamine Receptor Responsible for the Inhibition of Sex–pheromone Production in *Plodia interpunctella*, *Internet Electron*, *J. Mol. Des*. **2002**, *1*, 37–51, http://www.biochempress.com.
[9] A. Hirashima, E. Kuwano, and M. Eto, Three Dimensional Receptor Surface Model of Octopaminergic Agonists for the Locust Neuronal Octopamine Receptor, *Internet Electron. J. Mol. Des*. **2003**, *2*, 274–287, http://www.biochempress.com.
[10] G. E. Kellogg, M. Fornabaio, D. L. Chen, and D. J. Abraham, New Application Design for a 3D Hydropathic Map–Based Search for Potential Water Molecules Bridging between Protein and Ligand, *Internet Electron. J. Mol. Des*. **2005**, *4*, 194–209, http://www.biochempress.com.
[11] A. J. Hopfinger and J. S. Tokarsi, *Practical Applications of Computer–Aided Drug Design*; in: P. S. Charifson, Eds. Marcel Dekker: New York, **1997**, pp 105–164.
[12] A. Hirashima, T. Eiraku, E. Kuwano, and M. Eto, Three–Dimensional Molecular Field Analyses of Agonists for Tyramine Receptor which Inhibit Sex–Pheromone Production in *Plodia interpunctella*, *Internet Electron. J. Mol. Des*. **2003**, *2*, 511–526, http://www.biochempress.com.
[13] T. Wang, X. Wang, W. Wang, A. Lisa, Hasvold, G. Sullivan, C. W. Hutchins, S. O'Conner, R. Gentiles, T. Sowin, J. Cohen, W. Z. Gu, H. Zhang, S. H. Rosenberg, and H. L. Sham, Design and Synthesis of *o*–trifluoromethylbiphenyl Substituted 2–amino–nicotinonitriles as Inhibitors of Farnesyltransferase, *Bioorg. Med. Chem. Lett*. **2005**, *15*, 153–158.
[14] L. Wang, N. H. Lin, Q. Li, R. F. Henry, H. Zhang, J. Cohen, W. Z. Gu, K. C. Marsh, J. L. Bauch, S. H. Rosenberg, and H. L. Sham, Synthesis of 1H–pyridin–2–one Derivatives as Potent and Selective Farnesyltransferase Inhibitors, *Bioorg. Med. Chem. Lett*. **2004**, *14*, 4603–4606.
[15] L. Wang, G. T. Wang, S. Wang, Y. Tong, G. Sullivan, D. Park, N. M. Leonard, L. Qun, J. Cohen, W. Z. Gu, H. Zhang, J. L. Bauch, C. G. Jakob, C. W. Hutchins, S. Vincet, K. Marsh, S. H. Rosenberg, H. L. Sham, and N. H. Lin, Design, Synthesis, and Biological Activity of 4–[(4–Cyano–2–arylbenzyloxy)–(3–methyl–3*H*–imidazol–4–yl)methyl]benzonitriles as Potent and Selective Farnesyltransferase Inhibitors, *J. Med.Chem*. **2004**, *47*, 612–626.
[16] L. L. Rokosz, C. Y. Huang, T. M. Stauffer, J. C. Reader, D. Chelsky, N. H. Sigal, A. K. Ganguly, and J. J. Baldwin, Surfing the Piperazine Core of Tricyclic Farnesyltransferase Inhibitors, *Bioorg. Med. Chem. Lett*. **2005**, *15*, 5537–5543.
[17] Cerius^2 Molecular Modelling Program Package, Molecular Simulations (Accelrys) Inc.: San Diego, CA 92121–3752. USA, http://www.accelrys.com/cerius2.
[18] S. L. Mayo, B. D. Olafson, I. Goddard, DREIDING: A generic force field for molecular simulations, *J. Phys. Chem*. **1990**, *94*, 8897–8909.
[19] J. Gasteiger and M. Marsili, Iterative Partial Equalization of Orbital Electronegativity: A Rapid Access to Atomic Charges, *Tetrahedron*. **1980**, *36*, 3219–3222.
[20] M. J. S. Dewar, E. G. Zoebisch, E. F. Healy and J. J. P. Stewart, AM1: A New General Purpose Quantum Mechanical Molecular Model, *J. Am. Chem. Soc*. **1985**, *107*, 3902–3909.

[21] S. Wold, In: *Chemometric Methods in Molecular Design*, Eds. van de Waterbeemd H, VCH, Weinheim, 1995, Vol. 2, pp 195–218.
[22] Y. Fan, L. M. Shi, K. W. Kohn, Y. Pommier, J. N. Weinstein, Quantitative structure–antitumor activity relationships of camptothecin analogues: cluster analysis and genetic algorithm–based studies, *J. Med. Chem.* **2001**, *44*, 3254–3263.
[23] A. Golbraikh and A. Tropsha, Beware of q^2!, *J. Mol. Graph. Mod.* **2002**, *20*, 269–276.
[24] A. Hirashima, Y. Shigeta, T. Eiraku, and E. Kuwano, Inhibitors of calling behavior of *Plodia interpunctella*, *J. Insect Sci.* **2003**, *3*, 4, http://insectscience.org/3.4/.
[25] T. Equbal, O. Silakari, G. Rambabu, M. Ravikumar, Pharmacophore mapping of diverse classes of farnesyltransferase inhibitors, *Bioorg. Med. Chem. Lett.* **2007** (In Press).

Biographies

abish Equbal has completed B. Pharm. at Faculty of Pharmacy, Jamia Hamdard, New Delhi, India. Then he moved to the Department of Pharmaceutical Science and Drug Research, Punjabi University, Patiala, Punjab, India, and pursuing the M. Pharmacy degree. His research interests include rational drug design, CADD, 3–D QSAR, docking, pharmacophore mapping, and synthetic work and published research paper in reputed journal.

Om Silakari is lecturer in the Division of Pharmaceutical Chemistry at Department of Pharmaceutical Science and Drug Research, Punjabi University, Patiala, Punjab, India. After obtaining a Ph.D. degree in Pharmacy from Dr. H S Gour University, Sagar, India. Dr. Silakari supervising many PG students in the field of QSAR, rational drug design, and synthetic chemistry and published research papers in reputed journal in the field of QSAR.

Muttineni Ravikumar is a scientist in GVK Biosciences, Hyderabad, India. He did his M. Tech from Department of Chemical Engineering, Andhra University, Vishakhapatnam, A.P. India. . His research interests include rational drug design, CADD, 3–D QSAR, docking, pharmacophore mapping, and synthetic work, and published research papers in the various reputed journal.